REPORT DOCUMENTATION PAGE	1	Form Approved OMB NO. 0704-0188

1. REPORT DATE (DD-MM-YYYY) 29-08-2014	2. REPORT TYPE Book Chapter	3. DATES COVERED (From - To) -

4. TITLE AND SUBTITLE
Near-Field Spectroscopy and Imaging of Single Nanoparticles

5a. CONTRACT NUMBER
W911NF-12-1-0076

5b. GRANT NUMBER

5c. PROGRAM ELEMENT NUMBER
206022

6. AUTHORS
Yohannes Abate

5d. PROJECT NUMBER

5e. TASK NUMBER

5f. WORK UNIT NUMBER

7. PERFORMING ORGANIZATION NAMES AND ADDRESSES
California State University - Long Beach
California State University Long Beach Foundation
6300 State University Drive, Ste. 332
Long Beach, CA 90815 -4670

8. PERFORMING ORGANIZATION REPORT NUMBER

9. SPONSORING/MONITORING AGENCY NAME(S) AND ADDRESS (ES)
U.S. Army Research Office
P.O. Box 12211
Research Triangle Park, NC 27709-2211

10. SPONSOR/MONITOR'S ACRONYM(S)
ARO

11. SPONSOR/MONITOR'S REPORT NUMBER(S)
60430-MS-REP.12

12. DISTRIBUTION AVAILABILITY STATEMENT
Approved for public release; distribution is unlimited.

13. SUPPLEMENTARY NOTES
The views, opinions and/or findings contained in this report are those of the author(s) and should not contrued as an official Department of the Army position, policy or decision, unless so designated by other documentation.

14. ABSTRACT

The purpose of this entry is to review nanoscale near-field imaging and spectroscopy of single isolated nanoparticles
and core–shell nanostructures using scattering-type scanning near-field optical microscopy
(s-SNOM). Few representative examples have been chosen from the authors research work that are either plasmon or phonon resonant, quantum dots (QDs) and coated core–shell nanoparticles.

15. SUBJECT TERMS
nanoparticles, core–shell nanostructures, scattering-type scanning near-field optical microscopy (s-SNOM), plasmons, phonons, quantum dots (QDs)

16. SECURITY CLASSIFICATION OF:			17. LIMITATION OF ABSTRACT	15. NUMBER OF PAGES	19a. NAME OF RESPONSIBLE PERSON
a. REPORT	b. ABSTRACT	c. THIS PAGE			Yohannes Abate
UU	UU	UU	UU		19b. TELEPHONE NUMBER 562-985-4912

Standard Form 298 (Rev 8/98)
Prescribed by ANSI Std. Z39.18

Report Title

Near-Field Spectroscopy and Imaging of Single Nanoparticles

ABSTRACT

The purpose of this entry is to review nanoscale near-field imaging and spectroscopy of single isolated nanoparticles and core–shell nanostructures using scattering-type scanning near-field optical microscopy (s-SNOM). Few representative examples have been chosen from the authors research work that are either plasmon or phonon resonant, quantum dots (QDs) and coated core–shell nanoparticles.

Editor Query Form

Journal title: Dekker Encyclopedia of Nanoscience and Nanotechnology, Third Edition
Author: Yohannes Abate
Article id: E-ENN3-120050582

The following queries have arisen during copy-editing your manuscript. Please provide an answer in the right-hand column below and on your proofs. Many thanks for your help.

Query No.	Query	Response
EDQ1	Please provide in-text call out for Fig. 3.	

Near-Field Spectroscopy and Imaging of Single Nanoparticles

Yohannes Abate
Department of Physics and Astronomy, Georgia State University, Atlanta, Georgia, U.S.A.

Abstract

The purpose of this entry is to review nanoscale near-field imaging and spectroscopy of single isolated nanoparticles and core–shell nanostructures using scattering-type scanning near-field optical microscopy (s-SNOM). Few representative examples have been chosen from the authors research work that are either plasmon or phonon resonant, quantum dots (QDs) and coated core–shell nanoparticles.

INTRODUCTION

One of the most fascinating phenomenon in material science is the role size plays in altering the optical responses of nanoparticles.[1] Emerging synthesis methods allow fabrication of nanoparticles with a specific size and shape, which enable to tailor their optical response for clearly defined applications.[2,3] Plasmon resonances of metal nanoparticles can be tuned by controlling their size.[4] The past decade has witnessed an explosion in the use of plasmonic metal nanoparticles for light localization and near-field enhancement applications such as surface-enhanced Raman spectroscopy (SERS) and metal-enhanced fluorescence.[5,6] A great deal of research has been focused on quantum dots (QDs) with an interest in being able to tune their optical properties for integrated optoelectronic devices upon existing silicon technology infrastructure. Significant tuning of their band gaps can be achieved as a function of reduced size.[7] Tuning optical and chemical properties by reducing the size of materials has tremendously extended the potential of nanoscience that has received a major research focus.

As the ability to synthesize smaller and smaller complex core–shell nanostructures improves, an increased need to detect and map these materials on the nanoscale with material and spectroscopic sensitivity is recognized.[8–10] Optical methods, in addition to being non-destructive and chemically specific, allow investigation of structure–property relationships, effects of size and geometry on light-induced resonant properties of nanostructures (such as absorption and scattering), and plasmon–plasmon interactions. Classical light microscopy allows the resolution of sample features down to about half the illumination wavelength (~250 nm in the visible). This limited resolution hinders single particle characterization and spectroscopic investigation. Scattering-type scanning near-field optical microscopy (s-SNOM) offers ultrahigh optical resolution that depends on the radius of curvature of the probe and not on the wavelength of light used.[11–14]

S-SNOM is typically based on an atomic force microscope (AFM), where the sharp metallic probe tip is illuminated by a focused laser beam. The tip functions as an antenna converting the illuminating radiation into a highly localized and enhanced near field at the tip apex. Owing to the near-field interaction between the tip and sample, the tip-scattered radiation is modified in both its amplitude and its phase, depending on the local dielectric properties of the sample. Interferometric detection of the backscattered light thus yields nanoscale-resolved amplitude and phase images, rendering the local, complex dielectric function of the sample. From the near-field images, the absorption and scattering properties, local structure, material composition, and the free-carrier concentration, can be derived. The focus of this entry is to give a brief description of s-SNOM followed by a summary of recent works on single nanoparticle imaging with s-SNOM in the frequency range UV–visible to mid-infrared.

DESCRIPTION

Background-free successful optical imaging with s-SNOM (shown in Fig. 1) relies on: 1) Artifact-free topographic mapping; 2) high harmonic demodulation using lock-in amplifier; and 3) interferometric detection of the demodulated signal.

Topography

One of the most important, yet least emphasized, advantages of s-SNOM is its ability to acquire topographic information simultaneously with optical images. Successful operation of s-SNOM, and optical image interpretation relay on quality topographic imaging, it is therefore crucial to insure artifact-free topographic image before acquiring optical images with s-SNOM.

In AFM, the force interaction between a sharp probe tip affixed to a flexible cantilever and surface is measured. A reflected laser from the back of the cantilever is focused

Dekker Encyclopedia of Nanoscience and Nanotechnology, Third Edition DOI: 10.1081/E-ENN3-120050582

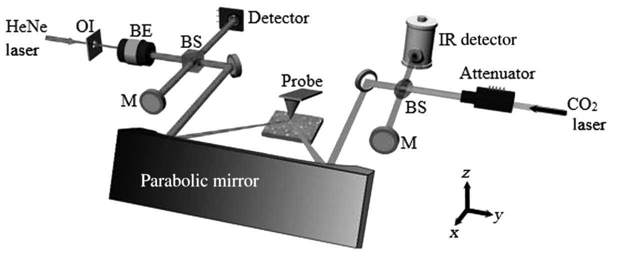

Fig. 1 Schematics of the experimental setup showing optical beam paths of the s-SNOM for visible (left side of tip) and infrared frequencies (right side of tip). M = mirror, OI = optical isolator, BE = beam expander, and BS = beam splitter.

to a detector, which translates the signal to a topographic image based on the vertical deflection of the cantilever. All s-SNOM is based on tapping mode AFM, because oscillation of the tip with near-resonant frequency is crucial to the optical near-field detection through high harmonic demodulation (described below). During tapping mode operation, the cantilever is allowed to oscillate at its slightly shifted resonance frequency with a free amplitude. A cantilever brought in close proximity to the surface taps the surface resulting in a decreased cantilever oscillation amplitude compared to the free amplitude. A feedback loop guarantees image formation through raster scanning over the sample surface and adjustments to the vertical displacement of the scanner.

High Harmonic Demodulation

Regular optical lens can focus a laser spot down to a micron diameter spot. When such a focused beam is directed to the AFM tip, it illuminates not only the desired tip apex but also the large portion of the shank of the tip and the sample surface. As a result the desired near-field signal is buried in the large unwanted "background" scattering coming from reflection from the shank of the tip and the sample surface. To extract the small near-field interaction, the signal is modulated at higher harmonics of the tip oscillation frequency using a lock-in amplifier. Because of the strongly anharmonic response of near-field signal with respect to the harmonic oscillation of the probe, compared to the nearly harmonic response of the scattered signal from the tip, this background term can be selectively removed by recording the signal at the higher harmonics (2Ω, 3Ω, ...) of the probe oscillation frequency.

Background reduction by harmonic demodulation becomes directly visible in approach curves such as those shown in Fig. 2. At the first harmonic frequency (ω) standing wave features that extend far beyond the near-field interaction zone dominate. These result from interference of different background contributions and may mask the expected near-field increase. With increasing modulation order (2ω, 3ω, 4ω…), however, the near-field contribution becomes clearly visible and even steepens, whereas the standing wave features are suppressed and are even lost in noise (Fig. 2). At small tapping amplitude (<50 nm) and large setpoint of the AFM feedback (>0.9), mechanical harmonics are negligibly small and so all the high harmonic signal comes from the optical near field. Taking approach curve measurements similar to the ones shown in Fig. 2 before taking s-SNOM measurements helps to fully exclude unnecessary contamination on the optical signal.

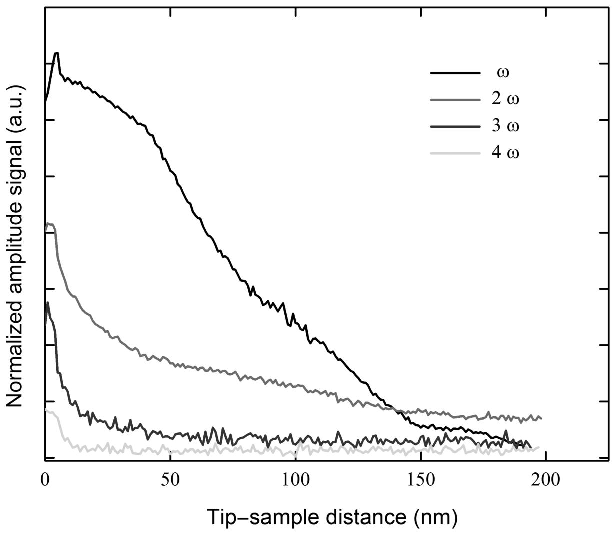

Fig. 2 Retraction curves at 1st, 2nd, 3rd, and 4th harmonics of resonance frequency of the probe.

Interferometric Detection

To amplify the weak near-field interaction signal modulated at higher harmonics of the tip resonance frequency, interferometric detection scheme is generally applied. Introducing interferometric detection with an external reference beam allows measurement of both the amplitude and the phase of the near-field scattering interaction, especially enabling near-field phase-contrast imaging. In pseudoheterodyne detection technique, the frequency shift is replaced by a sinusoidal phase modulation of the reference wave.[15] It offers the advantage of requiring only one beam splitter and a vibrating mirror in a Michelson interferometer configuration. It is much easier to implement than a heterodyne setup. Also, the needed components are readily available over the entire near-UV to far-IR spectral range. Furthermore, piezoelectric actuators drive the mirror with kilohertz frequencies and thus leave the useful signal in the submegahertz range where light detectors offer higher signal-to-noise ratio compared to detectors required by other interferometric techniques.

Theoretical Models

Few analytical models exist that predict tip–sample interaction when small particles are probed by s-SNOM. One of

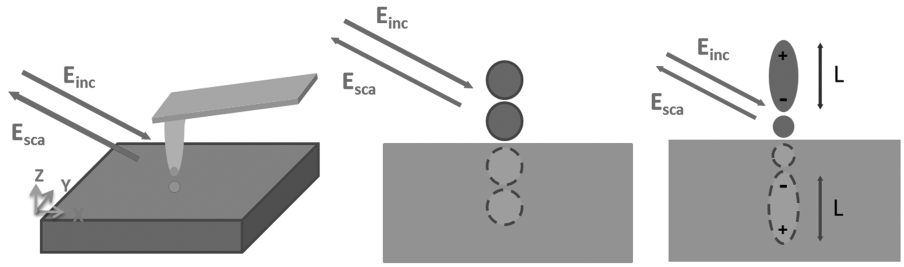

Fig. 3 Schematics of the finite-dipole where the tip is approximated by a spheroid in a uniform electric field and the point-dipole model where the tip is substituted by a point dipole located in a sphere at tip apex.

EDQ1

which is a model based on theoretical work of Gozhenko, Grechko, and Whites,[16] which relays on an analytical solution of the electrostatic boundary-value problem that takes into account the effect of the substrate for a system of spherical particles. For the special case of a system of two spheres above a substrate, an analytical expression for the sphere's polarizability is possible in the dipole approximation. In this approximation, the extreme end of the probe tip and the nanoparticle are considered as point dipoles interacting with their own image dipoles generated by the sample surface. The model is further based on the assumption that the line connecting the centers of the spheres is perpendicular to the substrate surface. When a nanoparticle is located between the probing tip and a flat sample the near-field amplitude signal is commensurate to the effective polarizability of the system of four dipoles, probe tip and the nanoparticle considered as point dipoles and their image dipoles generated by the sample surface. The effective polarizability is then calculated as the sum of the polarizability tensor of the tip and nanoparticle.

Alternatively a finite-dipole model is proposed to calculate the s-SNOM amplitude and phase contrast of particles smaller than the tip apex.[17,18] In this model the scattered field $E_{sca} = \sigma E_{in} = se^{i\varphi}\ E_{in}$; is described by the complex-valued scattering coefficient σ; derived from the near-field interaction between the illuminated tip and a flat semi-infinite substrate. The near-field probe is approximated by an isolated metal spheroid located in a uniform electric field. The spheroid is then reduced to a finite dipole p_0, which consists of the charges Q_0 and $-Q_0$, of which only Q_0 (positioned closer to the sample surface) participates in the near-field interaction. Because of the interaction between Q_0 and the sample surface, an additional point charge Q_i is induced close to the spheroid focus, whereas the opposite charge $-Q_i$ is distributed along the spheroid. The charges Q_i and $-Q_i$ form a finite dipole p_i, which describes the scattering from the spheroid that is induced by its near-field interaction with the sample surface. The scattered field is obtained by calculating $E_{sca}\ \alpha p_i E_{in}$. Assuming a sinusoidally varying tip–substrate distance at frequency Ω, the model yields the time course of the scattered field $E_{sca}(t)$. By Fourier transformation, we subsequently obtain the nth amplitude and phase coefficients, sn and φ_n. We have employed both the dipole and the finite dipole models to understand experimental data as described below.

NEAR-FIELD SPECTROSCOPY AND IMAGING OF SMALL NANOPARTICLES

Nanoscale Subsurface- and Material-Specific Identification of Single Au, SiO_2 and Hybrid Au/SiO_2 Nanoparticles

Au, SiO_2 capped Au and pure SiO_2 nanoparticles offer an excellent sample platform for a comprehensive review of s-SNOM near-field spectroscopy and imaging of small nanoparticles. Plasmonic and strong material contrast is provided by the Au nanoparticles (AuNPs) in the visible spectrum. In the infrared spectrum, SiO_2 provides near-field phonon spectroscopic investigation of small particles owing to Si–O stretch frequency accessibility in the range 9–11 μm. A hybrid SiO_2–Au nanoparticles allow a combined spectroscopy and near-field interaction investigation of phonons and plasmons, allow substrate-enhanced contrast and subsurface imaging. The SiO_2 coating also offers excellent layer uniformity while protecting nanoparticles from aggregation.

Employing s-SNOM direct investigation of the near-field optical contrast mechanism is presented by imaging the three types of individual particles (SiO_2, Au, and SiO_2-capped AuNPs) each on a Si substrate. Identification of capped and uncapped nanoparticles with nanoscale spatial resolution is demonstrated by imaging the mixture of the three types of nanoparticles adsorbed on the same Si substrate. An increased optical contrast between SiO_2 and SiO_2-capped AuNPs is observed in the visible spectrum. The strong tip–substrate coupling allow to distinguish SiO_2-capped AuNPs from bare SiO_2 particles because of the dipolar plasmon resonances of AuNPs underneath the SiO_2 coating layer near 633 nm. The plasmon-enhanced near-field coupling between the tip's near-field and the Au core through the SiO_2 cover layer enhances the weak near-field interaction of the SiO_2 capping layer. This additional signal strength, offered by the coupling to the Au core, results in a brighter contrast (larger amplitude) of the capped particle at lower tapping amplitude of the probing tip compared to a bare SiO_2 nanoparticle.

Such nanoscale resolution identification of mixed nanoparticles is well demonstrated in Fig. 4 which shows topography and near-field optical images of a mixture of three types of particles (SiO_2, Au, and SiO_2-capped AuNPs) on a Si substrate at a laser wavelength of, $\lambda = 633$ nm. In the topography image (Fig. 4A) all particles look identical while the optical amplitude image shows that the nanoparticles exhibit three different image contrasts compared to the substrate. Particles appear either bright, dark, or medium compared to the Si substrate. In Fig. 4C,D a zoomed-in image of the three contrast types captured in a 500 nm × 500 nm area is shown. Line plots of AFM heights (Fig. 4E) and optical amplitude signals (Fig. 4F) of two selected particles in Fig. 4C,D show that the heights of the two particles are the same ~50 nm (Fig. 4E). However, the amplitude signals differ (Fig. 4F), which suggests that the two particles are not the same type in the mixture composed of SiO_2, Au, and SiO_2-capped AuNPs. Furthermore, in Fig. 4D the brightest central particle which has a normalized amplitude signal of $s\ (s = sAu/sSi)$ ~3:1, is easily identified as Au as it is well known. Near-field interaction of the probing tip is expected to be stronger with the SiO_2-capped AuNP than with a bare SiO_2 particle due to a strong plasmon-enhanced coupling of the tip near field with the buried AuNP below the coating. These observations could suggest that the red line represents a SiO_2-capped AuNP and the blue line a bare SiO_2 particle.

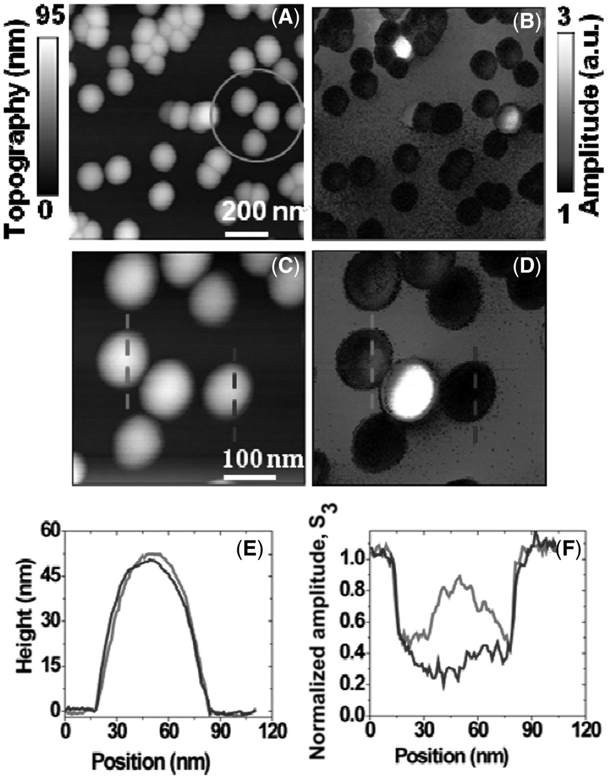

Fig. 4 Near-field images of a mixture of three types of nanoparticles: silica, Au, and silica-capped AuNPs absorbed on a Si substrate. (A) AFM topographic image of the mixture and (B) third harmonic $s3$ near field amplitude image. (C,D) High resolution zoom in scan results of the three particle types shown in green circle in (A) in a 500 nm × 500 nm area, (C) topography, and (D) third harmonic $s3$ near-field amplitude. (E) Line profiles of the topography of nanoparticles (red and blue dashed lines) showing similar height of the two particles. (F) Different optical signal line profiles for the two particles shown in red and blue dashed lines. Amplitude signal line profiles shown in (F) are normalized to the signal of a Si substrate.

An experiment performed on two samples containing only either SiO_2 nanoparticles or SiO_2-capped AuNPs adsorbed on Si substrate also confirm the above hypothesis that the signal contrast on capped particles is brighter than those on bare SiO_2 particles because of the plasmonic buried Au nanoparticles. The images used for analysis on these samples were acquired using the same scanning parameters, the same scanning tip, and the same tip vibrational amplitude. We performed pixel-by-pixel analysis of the data on each sample by correlating topography and near-field signal.[19] This is done by plotting the optical signal amplitude $s_3,(x,y)$ measured at a pixel (x,y) versus the height $h(x,y)$ extracted from the corresponding topography image on each nanoparticle. The result of the analysis is plotted in Fig. 5, which shows the bare SiO_2 containing sample in blue and the capped sample in red. For capped particles (red points), amplitude signal contrast values recorded at pixels near the center of the particles, which correspond to larger height values, are brighter than those farther from the center. These results support our hypothesis that the signal contrast on capped particles are brighter than those on bare SiO_2 particles, thus allowing identification of particles based on their material contrast.

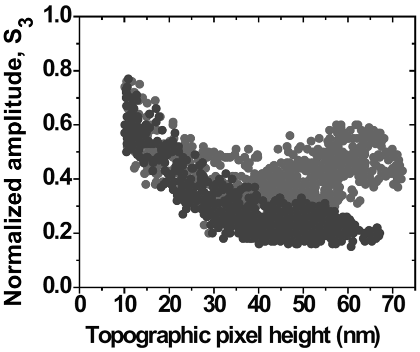

Fig. 5 Pixel-by-pixel correlation of measured near-field third harmonic signal contrast as a function of the topographic pixel height at 633 nm wavelength recorded for two samples, pure silica (blue data points) and silica-capped AuNPs (red data points) adsorbed on a Si substrate. Signal values on Si substrate are used to normalize all optical data.

The experimental results are supported by theoretical calculation using an extended dipole–dipole coupling model described above. The theoretical calculation agrees excellently with the experimental average data points. Capped and uncapped particles are identical in the size range when the height of the capped particle is less than the total thickness of capping layer (13 nm), and result in an overlapping amplitude signal until up to 26 nm particle height. As the core AuNP increases in size, the amplitude signal of a capped SiO_2 particle becomes stronger than a bare SiO_2 nanoparticle of the same size. The broad plasmon resonance of AuNPs in the visible[20] (expressed by the negative real part of the dielectric constant of Au)[21] results in resonant tip–substrate interaction that enhances the near-field contrast of the capped particles.[22] The increasing signal level with size is due to the increasing plasmon-enhanced near-field coupling between tip's near field and the AuNP core below the SiO_2 capping layer. The weak near-field interaction of the SiO_2 capping layer is therefore augmented by the strong near-field interaction of the embedded AuNP. This additional signal strength offered by the plasmonic Au core results in a brighter contrast (larger amplitude) of the capped particle compared to a bare SiO_2 nanoparticle of the same size.

Nanoscale Near-Field Infrared Spectroscopic Imaging of SiO_2-Shell/Au-Core, and Pure SiO_2 Nanoparticles

The work on near-field imaging of single SiO_2-shell/Au-core and pure SiO_2 nanoparticles in the infrared ($\omega =$ 9–11 μm) is the first study on spectroscopic imaging of thin coating layers and complex core–shell nanoparticles by s-SNOM. By tuning the wavelength of the incident light, information on the spectral phonon–polariton resonant near-field interactions of the SiO_2-shell/Au-core and pure SiO_2 nanoparticles with the probing tip was obtained. The enhanced near-field coupling between the high index Au-core and the probing tip achieves spectral near-field contrast of the thin SiO_2 coating (thickness ~10 nm). The sensitivity of s-SNOM imaging is known to improve if the sample of interest (e.g., nanoparticles or thin films) is placed on substrates with a high refractive index (e.g., Si or Au) due to near-field coupling between the tip and substrate.

Strong phase contrast is observed in capped particles with a thin SiO_2-shell, which is comparable to pure SiO_2 particles of similar height, near the wavelength where near-field phonon resonant interaction between the SiO_2-shell and the probing tip is expected. This is because of the enhanced near-field interaction of the probing tip with the high index Au-core in the capped particles.

The nanoscale optical properties of a homogeneous flat sample surface located below the illuminated tip, the scattered light and thus the near-field optical image contrast can be explained by approximating the probe as a dipole located at the tip apex. The near-field interaction between the tip dipole and its mirror image in the sample result in amplitude and phase signals of the scattered light that depend on the local dielectric function of the sample. If the sample exhibits infrared vibrational resonances, s-SNOM optical images can be considered as the resonant near-field interactions between the sample surface and the probing tip. The SiO_2 nanoparticles considered in this work have optical phonon frequency in the mid-IR, the characteristic near-field contrasts stem from a phonon–polariton resonant near-field interaction (which peaks starting around $\omega \sim 1000\ cm^{-1}$) between the probing tip and the SiO_2 sample surface. In capped nanoparticles, the dielectric function of the hybrid core–shell nanoparticle (SiO_2-shell/Au-core) is included in the simulation as a single dielectric function taken from Fofang et al.[23] and Wiederrecht, Wurtz, and Hranisavljevic[24] that includes the dielectric constant of the metal core and the dielectric constant of the SiO_2-shell. The dielectric function for the SiO_2 layer is described by a simple damped harmonic oscillator as described by Huber, Wittborn, and Hillenbrand[25] the model is further improved by taking into account the tip vibration amplitude (~20 nm) and signal harmonic demodulation to simulate experimental conditions. The demodulated second-harmonic signal is numerically calculated by Fourier transforming the modulated effective polarizability. Fig. 6 shows stronger amplitudes and phase signals at $\omega = 1080\ cm^{-1}$ near SiO_2 resonant tip–particle phonon–polariton interaction is expected and that at $\omega = 952\ cm^{-1}$ where such interaction is not expected. In general, for a given diameter of a particle an increasing amplitude and phase signals are observed at longer wavelengths close to SiO_2 phonon resonance. This is due to the increasing resonant tip–particle phonon–polariton interaction.

Both our experimental and theoretical calculation results for pure SiO_2 particles show a similar increasing trend toward lower wavelength as reported by Huber, Wittborn, and Hillenbrand[25]. The pure SiO_2 particles and the SiO_2-shell/Au-core particles result in a higher phase contrast at higher frequency ($\omega = 1000\ cm^{-1}$) where phonon resonant tip–particle interaction is expected. Owing to the correlation of the near-field-phase spectra with absorption spectra the strong phase contrast observed at higher frequency for the pure particles is not surprising. However, for capped particles the SiO_2-shell is only ~10 nm thick and still exhibits comparable phase contrast as pure particles at higher frequencies. This is because of the strong near-field interaction of the probing tip with the high index Au-core in the capped particles. The use of a metallic substrate such as gold for infrared wavelengths enhances the spectroscopic near-field signals of a vibrational fingerprint of the thin sample layer. This is due to the strong reflection of the incident radiation at the substrate that enhances the tip illumination and the enhanced tip–substrate near-field interaction further increases the local field acting on very thin sample layers (thickness <25 nm) thereby enhancing the near-field

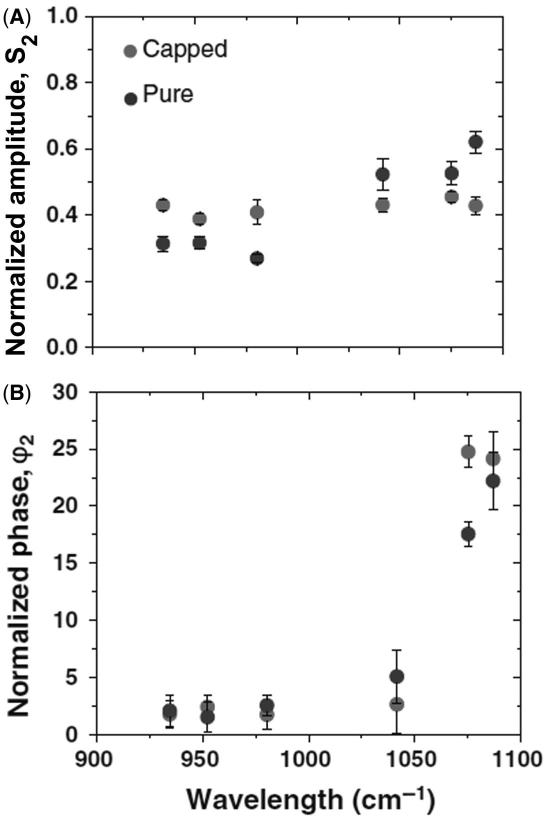

Fig. 6 Second harmonic demodulated near-field amplitude and phase spectra of silica capped-Au and pure silica nanoparticles on a silicon substrate. Red points represent results for silica capped Au nanoparticles and blue points represent results for silica nanoparticles, (A) experimental amplitude $s2$, with error bars (B) experimental phase spectra with error bars. All values are normalized to that of the Si substrate.

phase signals: which is a manifestation of the absorption spectra. Although the thin SiO_2-shell in the capped particles contains less-absorbing material compared to that of a pure SiO_2 particle, the strong near-field interaction of the Au-core with the metallic tip allows the capped particles to exhibit strong phase contrast. Substrate-enhanced s-SNOM allows spectroscopic identification of nanocomposites with nanometer resolution. This capability of s-SNOM should lead to the investigation of several important problems related to self-assembled monolayers, thin oxide layers, photoresists, and coatings.

CTAB Capped Au Nanoparticles

It is interesting to compare s-SNOM studies of the effect of organic capping agent CTAB and SiO_2 capping layers on the scattering properties of single metallic nanoparticles. The optical images obtained for uncapped gold particles reveal stronger ANSOM signals (on average stronger by 30% compared to the uncapped signal) compared to the capped particles of the same total height (gold plus capping layer) similar to SiO_2 capped Au particles discussed above. A capped particle of the same height as an uncapped one has a smaller gold nanoparticle at its center. The total effect is due both to the reduced size of the gold nanoparticle and the displacement of the s-SNOM tip and the displacement of the gold particle from the supporting substrate due to the spacer layer.

In this work, the experimental data of the effects of gold particle size and capping agent spacer layers on the near-field optical signals were best interpreted using a theoretical model that was developed. The model is based on an analytical solution of the electrostatic boundary-value problem that takes into account the effect of the substrate for a system of spherical particles.[16] For a system of two spheres above a substrate, an analytical expression for the sphere's polarizability is possible in the dipole approximation. Similar to the work in SiO_2 capped Au samples, the end of the probe tip and the nanoparticle are considered as point dipoles interacting with their own image dipoles generated by the sample surface. The calculations were done using the dielectric constant of the gold nanoparticle and the Si substrate used are $\varepsilon_{NP} = -11.8 + 1.25i$ and $\varepsilon_{Si} = 15.1 + 0.16i$, respectively, at 633 nm.[26] The model results gave excellent guidance to interpretation of the experimental data. It indicated that a capping spacer layer decreases the near-field coupling signal of a capped nanoparticle due to three different reasons. First, it increases the separation between the scattering tip and the nanoparticle by an amount proportional to the thickness of the layer. Second, it displaces the nanoparticle from the substrate also by an amount proportional to the layer thickness. Third, the gold nanoparticle embedded in the capping layer is smaller than the uncapped gold nanoparticle of the same height to which it is compared. It was also possible to estimate the spacer layer dimension by application of the theoretical model to the data, which assumes the embedding organic layer to be a transparent spacer layer in a first approximation. The calculations also indicated that the tip–nanoparticle separation and nanoparticle–substrate separation caused by the capping agent are each important in causing near-field signal reduction, while the tip–nanoparticle separation is a stronger effect.

The experiments with the CTAB capped particles were much harder with the results showing significant signal fluctuations. This is partly because of the lack of thickness uniformity of the CTAB coating layer. The SiO_2 coating overcame this difficulty and resulted in extensive near-field investigation and identification of capped and uncapped particles in a mixed sample that contain Au, SiO_2 capped/Au and pure SiO_2 nanoparticles. The high sensitivity of the change in scattered signal in s-SNOM opens the possibility to predict quantitative layer thicknesses of capping agents on the surface of nanoparticles, as well as the effect of capping layers on the optical scattering properties of nanoparticles.

Nanometer-Scale Dielectric Constant of Ge Quantum Dots

Nanoscale spectroscopic mapping of band gap properties of individual QDs and not ensemble averages, is challenging owing to the small size requirements of carrier confinement. Studies on single QDs can be performed by utilizing a widely tunable visible laser to interact with the tip of the s-SNOM situated over individual dot features. By interacting the s-SNOM tip with single QDs supported on a substrate, the dielectric properties and the effect on the s-SNOM signals around the vicinity of the band gap can be probed in detail.

In this work nanometer scale dielectric constant mapping of single Ge QDs grown on a Si substrate is introduced using s-SNOM. Two kinds of Ge QDs (dome shaped and pyramid shaped)[27] were grown on a Si substrate using an ultrahigh-vacuum chemical vapor deposition system at high temperature (800°C). To cover the peak spectral position of the QDs several CW lasers have been used in the range 1.5–3.1 eV, which include a violet diode laser (3.06 eV), an Ar ion laser (2.50 and 2.60 eV), a frequency-doubled Nd:YAG laser (2.33 eV), a Nd:YAG pumped tunable dye laser employing Rhodamine 6G (2.10 eV), a HeNe laser (1.96 eV), and a Ti:sapphire laser (1.55 eV). The use of several independent light sources to cover this spectral region makes the experiments very challenging. Recently, with the advent of broadband light sources that allow spectroscopic imaging using FTIR s-SNOM techniques have provided a means to overcome such challenges.

The main experimental results are summarized in Fig. 7, which shows the near-field spectral response of single Ge QDs, normalized to the Si substrate, at laser frequencies indicated above. From the topography images we note that typical base and height sizes of Ge QDs are 270 and 40 nm for dome shape and 220 and 21 nm for pyramid shape, respectively. Each spectral point in Fig. 7 is extracted from a topographical and optical images acquired at each laser frequency with the dome shape shown in solid circles and pyramidal ones in open circles. Since the spectral contrast is formed due to the tip near-field coupling to the Si substrate and the QD, it is necessary to normalize the near-field scattering intensity of single Ge QDs, to the Si substrate, for various wavelengths of the incident light. We used the average value of the scattering intensity of 10–20 individual QDs to normalize by that of the intensity of the Si substrate at that wavelength.

The normalized scattering intensity spectra show that Ge QDs are 2.86 times as large in contrast as that from Si substrate at 2.11 eV, which result in brighter contrast on amplitude image. However, at 3.10 eV the contrast of the scattered light images is darker than the substrate. Such contrast reversal can be observed because of size effect regardless of the dielectric constant of the sample as shown for both Au nanoparticles and SiN particles. The Ge Qds considered here are much larger in lateral dimensions and the contrast reversal observed is a direct effect of the difference in dielectric constant between the sample and the substrate. The amplitude image is proportional to the Re(ε), therefore the smaller Re(ε) of the Qd at 3.1 eV and larger Re(ε) at 2.11 eV relative to Si will result in a darker and brighter contrasts, respectively.

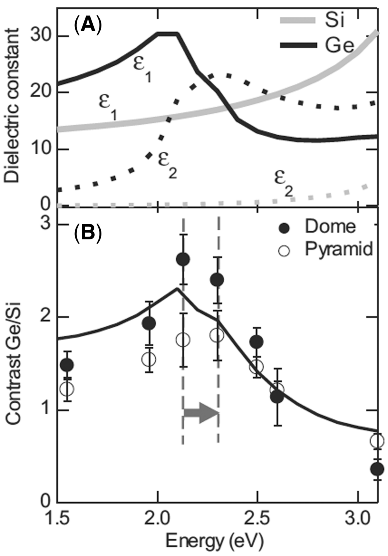

Fig. 7 (A) Dielectric constant of bulk Si (gray lines) and Ge (black lines). ε_1 is the real part (solid lines), ε_2 is the imaginary part (dashed lines). (B) Experimentally and theoretically obtained scattering intensity, normalized to the Si substrate, for dome and pyramid type dots.

The contrast of dome-shaped QDs is 1.3 times as large as that of pyramidal shaped ones. This is because the penetration depth of the optical near field is 30–50 nm, comparable to the height of the QDs. This results in enhanced tip near-field coupling with the dome-shaped QDs compared to the pyramidal-shaped ones owing to bigger size effect in the case of the dome-shaped structures since. In general, larger size can result in strong contrast due to proportionality of amplitude signal to the height of the QDs.

The normalized scattering intensity from Ge QDs is broad and dependent on the wavelength of the incident light peaking around 2.0–2.5 eV for both of the structures. Knowledge of the amplitude signal in s-SNOM offers direct information on the real part of the dielectric function of the sample as it is evident in the similarity of the normalized amplitude signal of Ge QDs to that of ε_1. The dielectric constants of bulk Si and Ge are mainly determined by the direct transition of Si in the UV region and by the El transition at the Ml saddle point of Ge in the visible region. The experimentally obtained spectral weight of the El transition in a single Ge QDs, which is shifted to higher energy of about 0.1 eV with decreasing the height. The pyramid-shaped structures are small enough in height to expect quantum confinement effects but the base size is too large for such an effect. Therefore, the observed blueshift is a result of the interplay between the quantum confinement effect and a compressive strain due to the lattice mismatch between the Ge QDs and the Si substrate by the Stranski–Krastanov growth.[27,28]

NANOSCALE INFRARED ABSORPTION SPECTROSCOPY OF INDIVIDUAL NANOPARTICLES

Chemical and structural specific analysis of thin films is routinely performed using absorption spectroscopy in the frequency region 400–4000 cm^{-1} (corresponding to wavelengths of 2.5–25 μm) also known as the fingerprint region. Far-field absorption experiments are constrained by diffraction limited spatial resolution and cannot allow investigation of individual nanoparticles and molecules. In this work it is shown that spectroscopic absorption vibrational finger print mapping of single 5 nm high nanoislands using s-SNOM phase measurements. The near-field phase spectroscopic measurements of the optical phonon–polariton mode of individual silicon nitride (Si_3N_4) nanoislands allow us to identify the Si–N stretching bond. A novel theoretical framework based on the near-field interaction between tip, sample, and substrate, were performed to show that the near-field phase spectra compare well with calculated far-field absorption spectra. The results establish that near-field phase spectroscopy allows far-field absorption spectroscopy of single nanoparticles where resolution is limited by the size of the probing tip and not by diffraction.

The Si_3N_4 particles were prepared on a cleaned Si wafer by annealing it in an ultra-high-vacuum chamber. The surface silicon oxide layer gradually decomposes, resulting in self-assembled silicon nanoislands which was exposed to nitrogen plasma which yields Si_3N_4 pyramidal-shaped nanoislands with varying heights below 10 nm.

Fig. 8 shows topography and simultaneously recorded IR amplitude s_2 and phase φ_2 images of the Si_3N_4 islands with heights ranging from 5 to 10 nm. Near-field amplitude s_2 and phase φ_2 images were recorded on and off the small-particle IR resonance of Si_3N_4 at 950 and 1050 cm^{-1}, respectively. The IR amplitude images at the two different frequencies show no significant change of the contrast between substrate and nanoislands. However, the near-field phase images exhibit a pronounced spectral contrast variation showing at 950 cm^{-1} a clear contrast between the Si_3N_4 particles and the substrate, which nearly vanishes at 1050 cm^{-1}. Typically, a spectral phase contrast in s-SNOM reveals an absorption in the sample, for example, caused by a vibrational resonance. Thus, the spectral phase contrast of the Si_3N_4 nanoislands indicates that we map the vibrational resonance of the Si–N stretching bond.

To ascertain this hypothesis the frequency-dependent near-field contrast between the Si_3N_4 nanoislands and the Si substrate were imaged at six different frequencies between 890 and 1100 cm^{-1}. Using nanoislands with heights of 5, 7, and 9 nm the phase φ_2 spectra shows a peak with a maximum at 930 cm^{-1}. Furthermore, the spectral amplitude contrast Δs_2 (Fig. 9A) and the spectral phase contrast $\Delta\varphi_2$ (Fig. 9B) decrease with decreasing height of the nanoisland. These experimental results are reproduced very well using a novel theoretical model based on the finite dipole approximation, where the scattered field $E_{sca} = \sigma E_{in} = se^{i\varphi}E_{in}$ is described by the complex-valued scattering coefficient σ is derived from the near-field interaction between the illuminated tip and a flat semi-infinite substrate. Using the dielectric function ε(ω) of Si_3N_4 the near-field amplitude s_2 and phase φ_2 spectra for Si_3N_4 spheres with diameters of 5, 7, and 9 nm were calculated. While the amplitude spectra (solid lines in Fig. 9A) are in good agreement with the experimental data and reveal typical s-SNOM amplitude spectra of a vibrational resonance, what is striking is the resemblance of the near-field phase spectra with the absorption spectra of small particles. To clearly establish this important correlation between near-field phase and far-field absorption spectra, particularly for nanoparticles, we calculate the far-field absorption cross-section of Si_3N_4 particles on a Si substrate. We assume an illumination polarization normal to the Si surface (i.e., grazing incidence). Taking

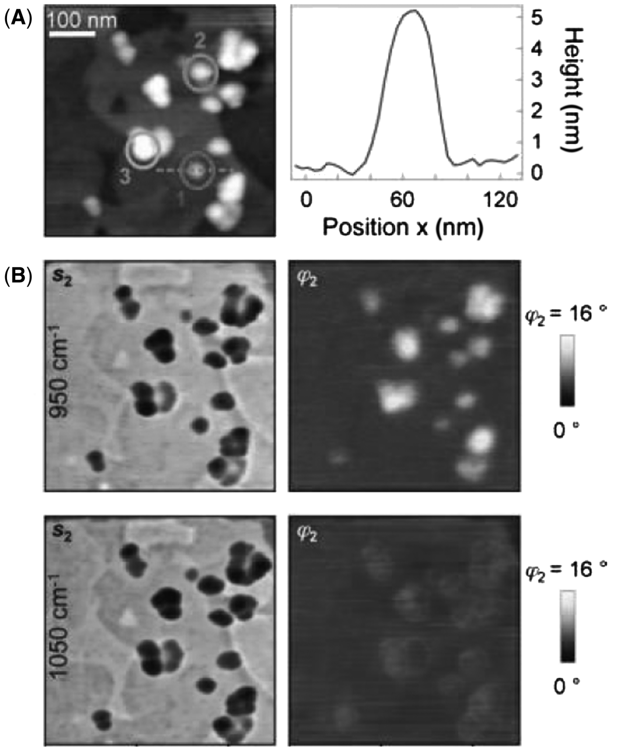

Fig. 8 Experimental images of Si_3N_4 nanoislands. (A) Topography as well as (B) IR near-field amplitude and phase at the two frequencies 950 and 1050 cm^{-1}. The line plot shows the height profile along the dashed orange line in the topography image.

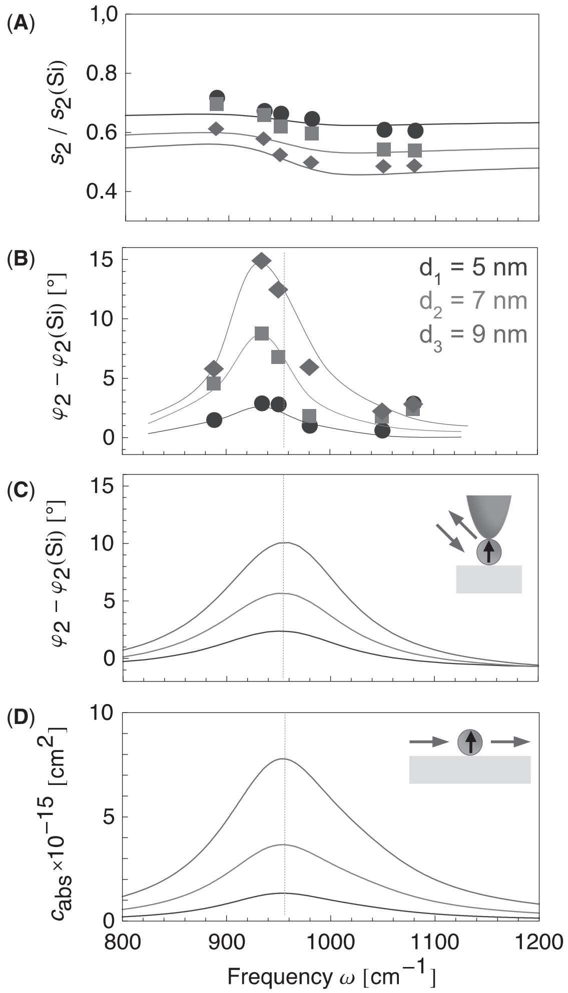

Fig. 9 IR spectral characteristics of individual Si_3N_4 nanoparticles. (a) Near-field amplitude. Experimental and (C) calculated near-field phase of particles. In (A–C), the particles are located on a Si substrate and both the experimental and the calculated data are normalized to the IR near-field amplitude, Si and phase, Si of the flat Si surface. (D) Calculated absorption cross-section of single Si_3N_4 nanoparticles on a Si substrate.

into account the influence of the substrate (coupling between particle dipole and its image dipole in the sample), we find for the Si_3N_4 particle a polarizability $\alpha^*_{Sphere} = \alpha_{Sphere}/[1-\alpha_{Sphere}\ (\varepsilon-1)(\varepsilon+1)^{-1}/(16\pi r^3)]$, yielding an absorption cross-section $C^*_{abs} = kIm[\alpha^*_{Sphere}]$.[18] In Fig. 9, we show C^*_{abs} for 5, 7, and 9 nm Si_3N_4 particles. Comparing the near-field phase signals φ_2 and the far-field absorption cross-section C^*_{abs}, we find that both exhibit the same qualitative spectral behavior. This clearly shows that the phase of the tip-scattered light reveals the absorption characteristic of small particles, despite the complex near-field interaction between tip, particle, and substrate. Fig. 9C shows the phase spectra φ_2 exhibit a good agreement with C^*_{abs}, the latter being the absorption cross-section of the particle on the substrate alone, i.e., in the absence of the tip. We thus conclude that the presence of the tip does not significantly modify the spectral signature of the particles.

To explore the sensitivity of s-SNOM, we measure the spectral IR amplitude and phase contrasts as a function of the Si_3N_4 particles height and also the signal above the Si substrate without a particle between tip and the Si surface. We find that for a given particle height, the amplitude is larger than the signal measured without a particle between tip and substrate because the presence of the Si_3N_4 particle enhances the near-field interaction between the tip and substrate. The measured phase contrast increases with an increasing particle height, while the measured phase signal on the Si substrate is constant independent of the tip–substrate separation. Calculations using the finite-dipole model reproduce the experimental data. The calculations also show that for particle height $h < 5$ nm both the amplitude and phase contrast vanish, thus challenging their experimental detection. The reason for the decreasing contrast of both the amplitude and phase contrast is the decreasing particle polarizability when the particle becomes smaller. Since the optical signal vanishing limit is determined by the size and the optical properties of the probing tip, using sharper tips with optimized antenna properties can push the detection limit further toward smaller particles.

This work demonstrates that the near-field spectroscopic detection of the IR spectrum of nanoislands with heights below 10 nm using an interferometric s-SNOM. The results show that near-field IR phase spectra of small particles exhibit a significant correlation to the far-field absorption. It can be understood by the fact that the dielectric properties of a material are complex-valued numbers, where the real part describes the refractive and the imaginary part the absorptive properties. The latter gives rise to a phase shift of the scattered light with respect to the incident light, which can be easily recorded by interferometric detection in s-SNOM. Thus, interferometric s-SNOM has the capability to map the IR absorption of materials with nanoscale spatial resolution.

SUMMARY

Spectroscopic investigation of single nanometer size particles and chemical characterization of complex core–shell nanoparticles are important in quality control for pharmaceutical or nanochemistry, photothermal therapeutic applications and detecting dopants and defect sites in single semiconductor nanoparticles. From the fundamental physics perspective such studies offer insight into the spectral near-field contrast of nanoparticles. Spectroscopic material-specific optical contrast imaging capability of nanoparticles down to a size of 5 nm combined with subsurface local imaging makes s-SNOM a very attractive tool for single particle studies and characterization.

The enhanced near-field coupling between the high index Au-core and the probing tip allows infrared spectroscopic near-field imaging of phonon resonant thin silica coating (thickness ~10 nm) in a silica-shell/Au-core nanoparticles. In the visible wavelength the strong plasmon– polariton–resonant tip–substrate coupling allow to distinguish silica-capped Au-core nanoparticles from bare silica particles. The plasmon-enhanced near-field coupling between the tip's near field and the Au core through the silica cover layer enhances the weak near-field interaction of the silica capping layer[18] allowing easier particle identification. The near-field detection of the IR spectrum of nanoislands with heights below 10 nm could be performed using interferometric s-SNOM. The near-field IR phase spectra of small particles exhibit a significant correlation to the far-field absorption. The imaginary part of the absorptive properties gives rise to a phase shift of the scattered light with respect to the incident light, which can be easily recorded by interferometric detection in s-SNOM. Spectroscopic s-SNOM near-field scattering images of Ge QDs fabricated on a Si substrate reveal a blueshift of the spectral dispersion of single QDs as the size is reduced.

ACKNOWLEDGMENTS

Financial support provided in part by the American Chemical Society, Petroleum Research Fund (ACS PRF) under grant PRF# 50461-UNI10, Research Corporation for Science Advancement Award and the U.S. Army Research Office, Agreement Number: W911NF-12-1-0076 are all gratefully acknowledged.

REFERENCES

1. Lance Kelly, K.; Coronado, E.; Zhao, L.L.; Schatz, G.C. The optical properties of metal nanoparticles: the influence of size, shape, and dielectric environment. J. Phys. Chem. B **2002**, *107* (3), 668.
2. Lu, X; Rycenga, M.; Skrabalak, S.E.; Wiley, B.; Xia, Y. Chemical synthesis of novel plasmonic nanoparticles. Ann. Rev. Phys. Chem. **2009**, *60* (1), 167.
3. Grzelczak, M.; Perez-Juste, J.; Mulvaney, P.; Liz-Marzan, L.M. Shape control in gold nanoparticle synthesis. Chem. Soc. Rev. **2008**, *37* (9), 1783.
4. Prashant, K.J.; Huang, X.; El-Sayed, I.H.; El-Sayed, M.A. Noble metals on the nanoscale: optical and photothermal properties and some applications in imaging, sensing, biology, and medicine. Account. Chem. Res. **2008**, *41* (12), 1578.
5. Anger, P.; Bharadwaj, P.; Novotny, L. Enhancement and quenching of single-molecule fluorescence. Phys. Rev. Lett. **2006**, *96* (11), 113002.
6. Nie, S.; Emory, S.R. Probing single molecules and single nanoparticles by surface-enhanced Raman scattering. Science **1997**, *275* (5303), 1102.
7. Segets, D.; Lucas, J.M.; Klupp Taylor, R.N.; Scheele, M.; Zheng, H.; Alivisatos, A.P.; Peukert, W. Determination of the quantum dot band gap dependence on particle size from optical absorbance and transmission electron microscopy measurements. ACS Nano **2012**, *6* (10), 9021.
8. Alivisatos, A.P. Semiconductor clusters, nanocrystals, and quantum dots. Science **1996**, *271* (5251), 933.
9. De, M.; Ghosh, P.S.; Rotello, V.M. Applications of nanoparticles in biology. Advanced Mater. **2008**, *20* (22), 4225.
10. Dong, H.; Zhu, M.; Yoon, J.A.; Gao, H.; Jin, R.; Matyjaszewski, K. One-pot synthesis of robust core/shell gold nanoparticles. J. Am. Chem. Soc. **2008**, *130* (39), 12852.
11. Keilmann, F.; Hillenbrand, R. Near-field microscopy by elastic light scattering from a tip. Philos. Trans. R. Soc. Lond. Ser. A Math. Phys. Eng. Sci. **2004**, *362* (1817), 787.
12. Hillenbrand, R.; Keilmann, F. Complex optical constants on a subwavelength scale. Phys. Rev. Lett. **2000**, *85* (14), 3029.
13. Novotny, L. Effective wavelength scaling for optical antennas. Phys. Rev. Lett. **2007**, *98* (26), 266802.
14. Kim, Z.H.; Leone, S.R. High-resolution apertureless near-field optical imaging using gold nanosphere probes. J. Phys. Chem. B **2006**, *110* (40), 19804.
15. Ocelic, N.; Huber, A.; Hillenbrand, R. Pseudoheterodyne detection for background-free near-field spectroscopy. Appl. Phys. Lett. **2006**, *89* (10), 101124.
16. Gozhenko, V.V.; Grechko, L.G.; Whites, K.W. Electrodynamics of spatial clusters of spheres: substrate effects. Phys. Rev. B **2003**, *68* (12), 125422.
17. Cvitkovic, A.; Ocelic, N.; Hillenbrand, R. Analytical model for quantitative prediction of material contrasts in scattering-type near-field optical. Opt. Express **2007**, *15* (14), 8550.
18. Stiegler, J.M.; Abate, Y.; Cvitkovic, A.; Romanyuk, Y. E.; Huber, A.J.; Leone, S. R.; Hillenbrand, R. Nanoscale infrared absorption spectroscopy of individual nanoparticles enabled by scattering-type near-field microscopy. ACS Nano **2011**, *5* (8), 6494.
19. Cvitkovic, A.; Ocelic, N.; Hillenbrand, R. Material-specific infrared recognition of single sub-10 nm particles by substrate-enhanced scattering-type near-field microscopy. Nano Letters **2007**, *7* (10), 3177.
20. Eustis, S.; El-Sayed, M.A. Why gold nanoparticles are more precious than pretty gold: noble metal surface plasmon resonance and its enhancement of the radiative and nonradiative properties of nanocrystals of different shapes. Chem. Soc. Rev. **2006**, *35* (3), 209.
21. Hillenbrand, R.; Taubner, T.; Keilmann, F. Phonon-enhanced light matter interaction at the nanometre scale. Nature **2002**, *418* (6894), 159.
22. Aizpurua, J.; Taubner, T.; Garcia de Abajo, F.J.; Brehm, M.; Hillenbrand, R. Substrate-enhanced infrared near-field spectroscopy. Opt. Express **2008**, *16* (3), 1529.
23. Fofang, N.T.; Park, T.H.; Neumann, O.; Mirin, N. A.; Nordlander, P.; Halas, N.J. Plexcitonic nanoparticles: plasmon–exciton coupling in nanoshell–J-aggregate complexes. Nano Letters **2008**, *8* (10), 3481.
24. Wiederrecht, G.P.; Wurtz, G.A.; Hranisavljevic, J. Coherent coupling of molecular excitons to electronic polarizations of noble metal nanoparticles. Nano Letters **2004**, *4* (11), 2121.
25. Huber, A.J.; Wittborn, J.; Hillenbrand, R. Infrared spectroscopic near-field mapping of single nanotransistors. Nanotechnology **2010**, *21* (23), 235702.

26. Hecht, B.; Bielefeldt, H.; Inouye, Y.; Pohl, D.W.; Novotny, L. Facts and artifacts in near-field optical microscopy. J. Appl. Phys. **1997**, *81* (6), 2492.
27. Baranov, A.V.; Fedorov, A.V.; Perova, T.S.; Moore, R.A.; Yam, V.; Bouchier, D.; Le Thanh, V.; Berwick, K. Analysis of strain and intermixing in single-layer Ge/Si quantum dots using polarized Raman spectroscopy. Phys. Rev. B **2006**, *73* (7), 075322–075327.
28. Teng, C.W.; Muth, J.F.; Kolbas, R.M.; Hassan, K.M.; Sharma, A.K.; Kvit, A; Narayan, J. Quantum confinement of E_1 and E_2 transitions in Ge quantum dots embedded in an Al_2O_3 or AlN matrix. Appl. Phys. Lett. **2000**, *76* (1), 43.